

Article

Characteristics and Control of Mining Induced Fractures above Longwall Mines Using Backfilling

Shuokang Wang ¹  and Liqiang Ma ^{1,2,*} 

¹ Key Laboratory of Deep Coal Resource Mining, Ministry of Education of China, China University of Mining & Technology, Xuzhou 221116, China; skwang@cumt.edu.cn

² School of Energy, Xi'an University of Science and Technology, Xi'an 710054, China

* Correspondence: ckma@cumt.edu.cn; Tel.: +86-0516-8359-0579

Received: 17 October 2019; Accepted: 2 December 2019; Published: 3 December 2019



Abstract: Water conservation in mining is the key to solving the conflict between coal resource exploitation and ecological environment protection, especially in arid and semi-arid mining areas. Continuous excavation and continuous backfilling (CECB) in longwall mining is an important method to realize water conservation mining. Considering the different boundary conditions of the main roof stress in different mining phases, the mechanical models of clamped–clamped beam, continuous beam, and elastic foundation beam among filling body, main roof, and strata are established. Furthermore, the spatio-temporal evolution mechanisms of mining-induced fractures (MIF) are studied. It is found that there is a hyperbolic function relationship between MIF and the mining roadway (MR) filling percentages. Based on mining the XV coal seam under CECB in the Wangtaipu Coal Mine, the distribution patterns of MIF are studied. It is concluded that the distribution pattern is an isosceles trapezoid with the moving angle of overlying strata as the bottom angle, and the upper and lower boundary of MIF as the two parallel sides. Based on the influence coefficient of MR filling percentages on MIF, the curve of the MIF height is divided into three ranges, which include the stability control range, the critical range, and the lost control range. The controlling effects of MR filling percentages are studied, and the calculation expression of the MIF height in the stability control range is given. In engineering practice, 90% MR filling percentage is used for CECB. The MIF height is about 3.0 times of mining height, and the main roof beam is not broken. The water-resisting property of aquiclude III is not destroyed, thus, the mining does not adversely impact the water. The results provide theories and practices for controlling MIF under CECB in the conditions of extremely close distance aquifers.

Keywords: water conservation mining; continuous excavation and continuous backfilling (CECB); mining induced fractures (MIF); mining roadway (MR); filling percentages

1. Introduction

China is the largest coal producing nation in the world. For the past decade, the average coal production in China is approximately 3.48 billion tons a year, which represents 43.81% of the total coal production in the world [1]. Coal has been a tremendous booster for China's economic development, but has also brought considerable negative impacts on ecological environment, especially on water resource. On the average, 2.04 m³ water should be discharged for producing a ton of coal [2–4]. Coal mining can cause the deterioration of regional ecological environment especially in arid and semi-arid mining areas which have vulnerable ecosystems [5,6]. Achieving the conservation of water resource in coal mining process is of great significance to maintaining ecological balance in the mines [7–10].

As early as the 1960s, with the aim of attempting the conservation of water resource in the coal mining process, Austrian scholars began to use tracer agents to examine the relation between subsidence and underground water [11]. American researchers investigated the strata disturbance

region while performing coal mining under a surface water, and established related mathematical models to predict water diversion performances of the mining-induced fractures [12,13]. Chinese scholars proposed the concept of water conservation mining from the end of the 20th century. After the development over the past 30 years, systematical water conservation mining technical and theoretical system has been initially established in China [14–17]. At present, the water conservation mining methods mainly include drift mining, slice mining (height-limit mining), room and pillar mining, and backfilling. Specifically, drift mining exhibits certain limitations, including low coal recovery rate and difficulty in recovery of stranded coal pillars; using slice mining (height-limit mining), the mining time and the effects on aquifer can hardly be determined; room and pillar mining also encounters some difficulties, such as low coal recovery rate and complex production processes. By contrast, the backfilling mining (also referred to mining with backfilling) becomes the most effective water conservation mining method; nevertheless, traditional longwall backfilling technology also shows some problems, such as insufficient constraints of backfilling space and great difficulties in mining activity coordination, thereby seriously restricting the development of water conservation mining [18–20].

In recent years, by combining the advantages and concepts of the Wongawilli rapid mining method [21,22] and pillar backfilling mining [23], the writers proposed continuous excavation and continuous backfilling (CECB) in longwall mining and explored the preparation of filling materials [24,25]. This method adopts the interval excavated MRs for coal mining. Once a MR is excavated, it will be filled immediately. At the same time, the next MR will be excavated until all MRs of the whole working face are excavated and filled, as shown in Figure 1. This method can successfully overcome the limitations in traditional longwall backfilling mining and provide the backfilling face with sufficient time and effective space. Accordingly, the filling bodies can be solidified, and the requirements on bearing strength can be satisfied to effectively control mining-induced fractures (MIF).

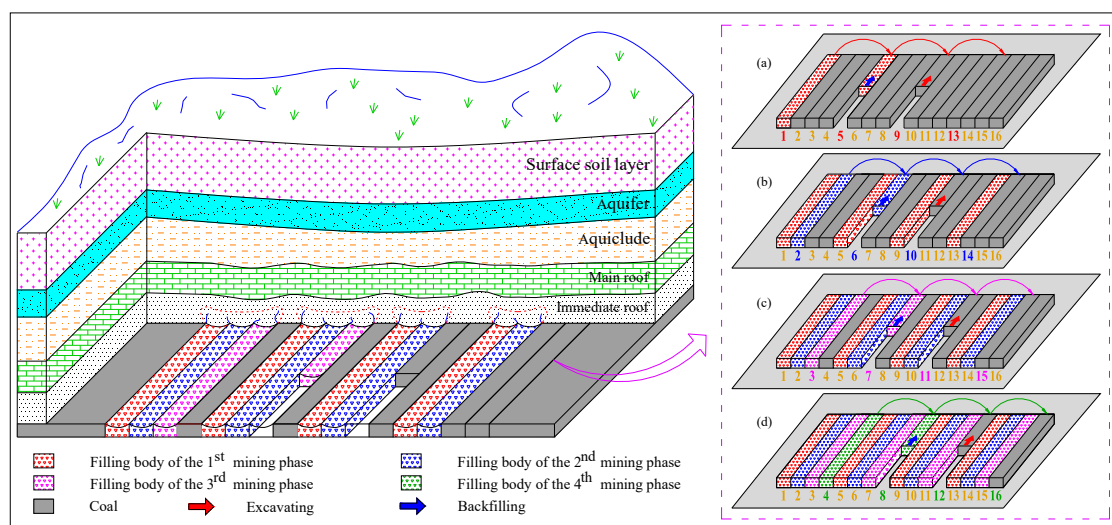


Figure 1. The schematic diagram of CECB coal mining process.

It is one of the important scientific problems in water conservation mining that avoiding MIF conducting through aquifers [26]. Scholars have undertaken considerable researches on the law of MIF and its influence on water resources when longwall mining. American scholars have studied the importance of aquicludes between aquifers and coal seam by studying MIF in longwall working face [27,28]. Ukrainian scholars studied the distribution pattern and evolution law of MIF in a longwall working face of the Donetsk coalfield, and divided the overlying strata into caving zone, fracture zone and continuous deformation zone [29]. At the same time, the caving zone and fissure zone were defined as MIF connected area of roof water. Chinese scholars have detected MIF distribution patterns of hundreds of longwall working faces under different geological conditions, and concluded that MIF in overlying strata are saddle shaped [30,31]. In addition, scholars have laid a theoretical foundation

for backfilling water conservation mining by studying the law of MIF under longwall backfilling and drift backfilling conditions [32,33].

However, there are relatively few studies on the control of MIF in roadway backfilling, especially the characteristics and control of MIF under CECB are still unclear. The interval mining technology under CECB leads to alternate distribution between coal pillar (or filling body) and mined roadway [34]. The supporting structures of strata are discontinuous, and the distribution patterns of MIF are also different. In addition, CECB is essentially a backfilling mining method. The main control principle of MIF is to fill before the goaf forms and occupy the subsidence space of strata, reduce the degree of strata migration, and control the development of MIF. The filling percentage is an important parameter to measure filling qualities and filling effects. Therefore, the control of MIF through the mining roadway (MR) filling percentages is one of the important scientific problems of CECB. At present, there is relatively little research in this area.

Based on the engineering background of CECB in the Wangtaipu Coal Mine, and on the basis of different boundary conditions of the main roof stress, this paper establishes the mechanical models of clamped-clamped beam, continuous beam and elastic foundation beam between the filling body, main roof, and strata. Moreover, the mechanism and characteristics of MIF are analyzed, and the controlling effects of filling rates on MIF are studied. The present results should provide theoretical and practical guidance for water conservation mining under extremely close distance aquifers and other practices of water conservation mining with extremely thin barriers.

2. Research Background

2.1. Profile of the Study Area

The Wangtaipu Coal Mine is located at the south of Shanxi, China, and its mining area is about 33.79 km². The residual recoverable reserves in this mine are approximately 57.46 Mt which are mostly deposited below buildings or water resources. To be specific, the XV23 mining segment has a mean depth of 220 m, a strike length of 330 m, a dip length of 156 m and the reserves of approximately 0.19 Mt. The under mining coal seam, namely XV coal seam, has a mean thickness of 2.38 m and a dip angle of 1~2°. Figure 2 displays the study area.

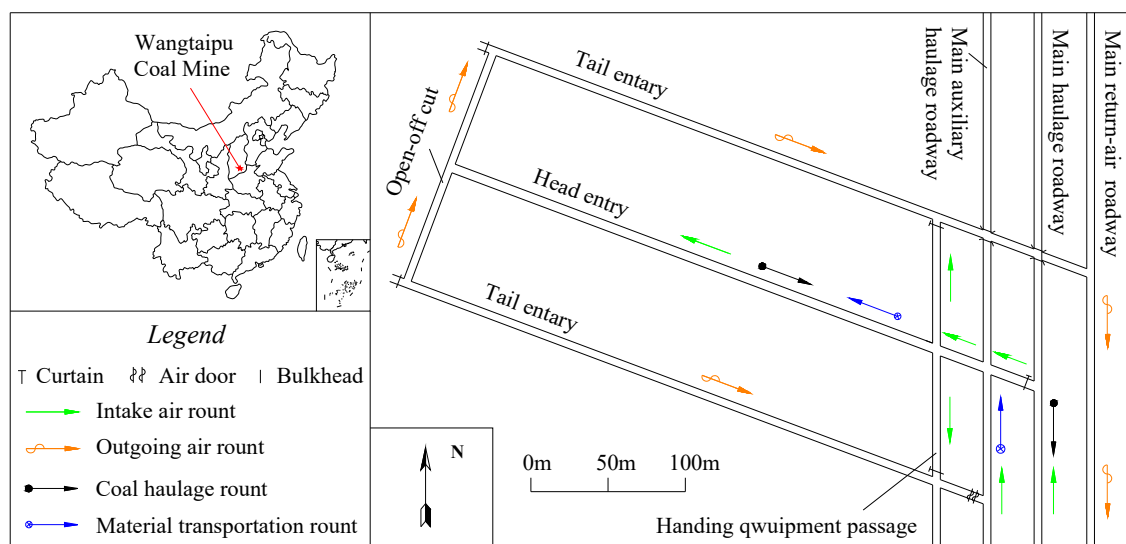


Figure 2. Schematic diagram of the study area.

2.2. Stratigraphic Structure

The XV coal seam is located in upper the Taiyuan formation of carboniferous system (C_{3t}), as the stratigraphic structure shown in Figure 3. The main roof of the coal seam is composed of limestone

with a mean thickness of 8.50 m, while the floor is composed of mudstone with a mean thickness of 9.40 m. The uniaxial compressive strength and Brazilian tensile strength of main are 101.6 MPa and 28.3 MPa, respectively, while the uniaxial tensile strength and the Brazilian tensile strength of main floor are 4.0 MPa and 1.4 MPa, respectively.

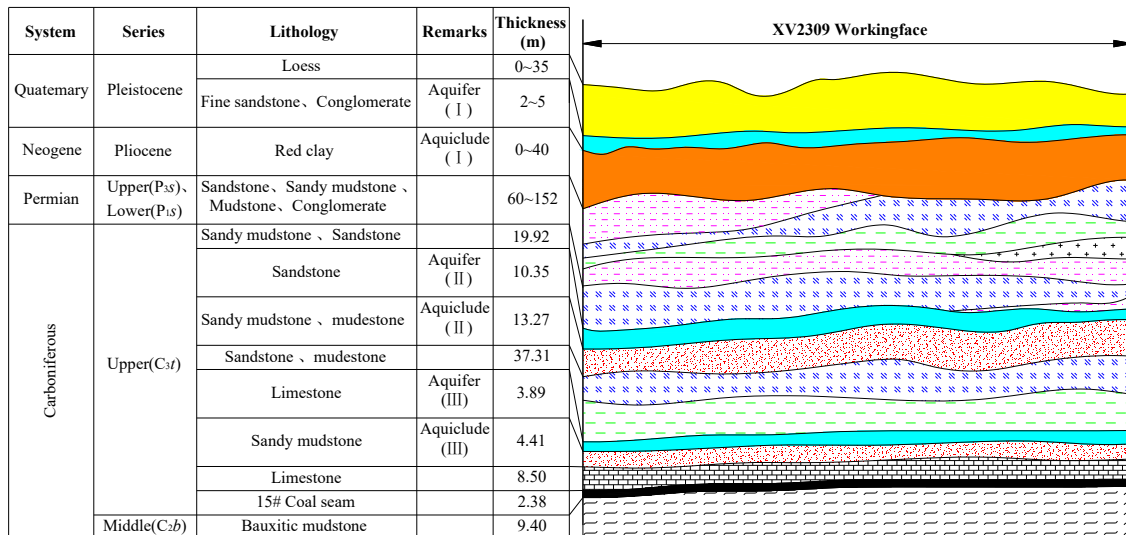


Figure 3. Stratigraphic structure of the study area.

In the stratigraphic structure, there exist three aquifers. Aquifer I is situated below the Quaternary yellow clay overburden with a thickness of 2~5 m. It is an aquifer with water supply significance and ecological value. Aquifer II is located near the boundary between Permian and Carboniferous, mainly consisting of 4~5 aquifer sandstones with a total thickness of about 10.35 m. Aquifer III locates approximately 13 m above the XV coal seam, with a mean thickness of 3.89 m, a normal water inflow of 1~3 m³/h, and a maximum water inflow of 10 m³/h.

2.3. Mining Method of CECB

Aquifer III is within the influence range of XV coal mining. If the caving mining is adopted, the aquifer will be within the range of overburden caving zone (8 times of mining height), which will inevitably cause the damage of aquifer, leading to the loss of water resources and water inrush into the working face. CECB (Figure 4) is an effective method to solve the problem of water conservation mining under extremely close distance aquifers.

CECB is a mining method of combining wall system mining technology with continuous and rapid room and pillar mining. According to longwall mining method, head entry, tail entry, and open-off cut are laid out [25]. Before excavating, the CECB working face is divided into n mining roadways (MRs), and MRs are divided into m (usually $m = 2\sim 5$) mining phases. During excavating, MRs are excavated in turn, and the excavated MRs are filled immediately. In the CECB working face, the “parallel excavating and filling” operation mode is always maintained, until all the MRs are excavated and filled.

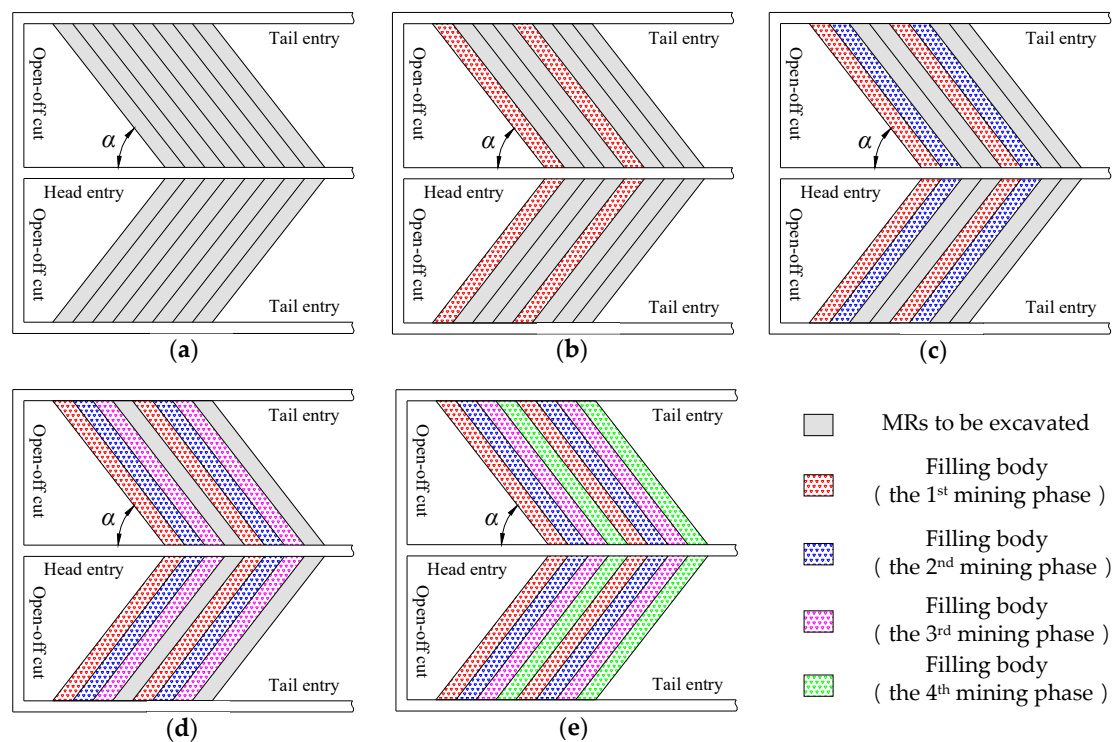


Figure 4. Main mining processes of CECB. (a) The layout of MRs; (b) filled the 1st mining phase MRs; (c) filled the 2nd mining phase MRs; (d) filled the 3rd mining phase MRs; and (e) filled the 4th mining phase MRs.

3. Development Mechanisms of MIF

Based on the stress characteristics of the main roof in different mining phases, the mechanical models of the clamped-clamped beam, continuous beam, and elastic foundation beam among the filling body, main roof, and strata are established. The deformation characteristics of the main roof in each mining phase are analyzed, and the expressions of the MIF height are given.

3.1. Mechanical Models

After the excavation of MRs, the main roof is subjected to the load of strata and the supporting effect of coal pillars on both sides of MR, forming a rock beam structure. After backfilling, the filling bodies act as cushion and supports the main roof synergistically, providing support for the rock beam structure. During excavation, the exposed area of the main roof and the length of beam in mining space are gradually enlarged. Although the rock beam structure of the main roof is continuous in space, the stress and subsidence of the main roof above the MRs of adjacent mining area are not continuous in time. The deformation of the main roof appears a cusp (non-differentiable point) at the junction of the adjacent MRs.

During the whole CECB, the main roof is a kind of rock beam structure which is always supported by the backfilling and the support resistance increases as mining progresses. However, with the increase of mining phase, the rock beam structure evolves gradually from clamped-clamped beam to continuous beam and then to elastic foundation beam. Figure 5 shows the mechanics models of clamped-clamped beam, continuous beam, and elastic foundation beam among the filling body, main roof, and strata in different mining phases.

3.1.1. Clamped–Clamped Beam Model

After the first mining phase, the coal pillars with a width three times that of the MR are isolated by MRs. According to the engineering practice experience, the interaction between the two MRs

should be ignored. It is considered that the influence of the excavating and filling MRs on the strata is independent [35]. In this phase, the coal pillar can provide fixed support constraint for the main roof, which can not only transfer stress, but also transfer bending moment at the constraint end. The stress characteristics of the main roof after the first mining phase are simplified to a clamped-clamped beam model, as shown in Figure 5a. In the figure, L_0 is the length of the beam which is equal to the width of the MR, q is the load on the strata which is simplified as a uniform distribution, and f is the supporting force of the filling body. The connecting joints marked 1 and 2 represent the fixed support constraint of the coal pillars on the main roof.

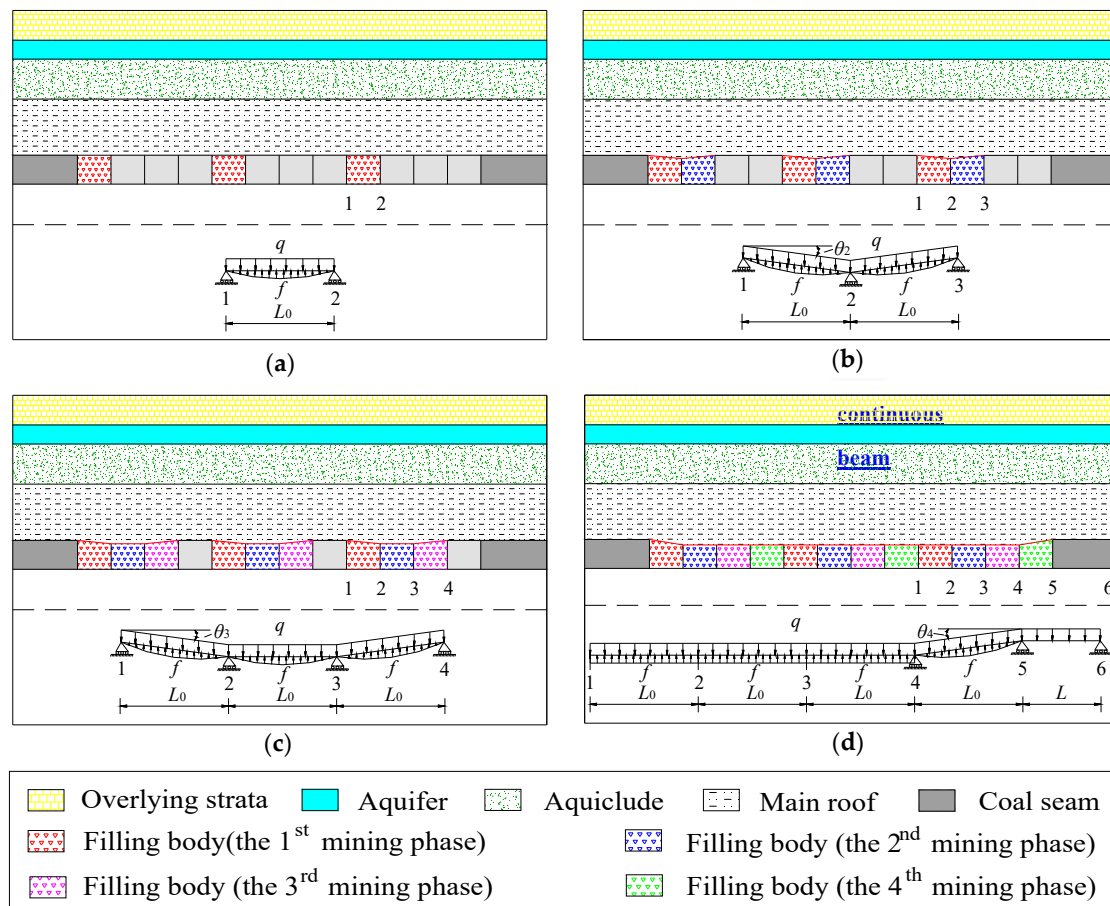


Figure 5. Stratigraphic structure of the study area. (a) Clamped-clamped beam model; (b) continuous beam model (one connecting joint); (c) continuous beam model (two connecting joints); and (d) elastic foundation beam model.

3.1.2. Continuous Beam Model

With the increase of mining, the exposed area of basic roof increases, and the structure of rock beam will change. In order to establish the mechanical model of the continuous beam, the following basic assumptions are made: (1) The mining technology of CECB can protect the main roof from breaking, which can always transmit stress and bending moment during the mining and filling. (2) Before the excavation of MR, the adjacent filling body has been fully compacted and in a stable state, which can replace the coal pillar to effectively support the main roof. (3) The connecting joint between the two MRs act as a fixing and restraining function to the main roof, and the angles of the main roofs on both sides of the point match each other (rotation angles are equal in size and reverse in direction) [36]. (4) Coal pillars can play a role of stress isolation, and the mechanical characteristics of the main roof can be simplified as a continuous beam structure with multiple intervals and independence.

The mechanical model of continuous beam is shown in Figure 5b,c. Figure 4b corresponds to the stress characteristics of the main roof after the second mining phase. The continuous beam model is connected by two equal-length clamped-clamped beams through connecting joint 2. The connecting joint 1 and connecting joint 3 are two fixed-supported ends and are on the same level. Due to the sinking of the main roof, the connecting joint 2 is lower than this level. In Figure 5b, the continuous beam model is asymmetrically distributed at connecting joint 2, and the 1–2 and 2–3 segments rotate θ_2 clockwise and counterclockwise, respectively.

Figure 5c corresponds to the stress characteristics of the main roof after the third mining phase, which is an extension of Figure 5b. The continuous beam model is composed of three equal-length clamped-clamped beams through connecting joint 2 and connecting joint 3. Connecting joint 1 and connecting joint 4 are two fixed-supported ends which are on the same level. In the process of forming the 3–4 segment, connecting joint 3 sinks with the main roof. According to the assumption of continuous beam model, it is advisable to simplify the 2–3 segment into horizontal ones. In Figure 5c, the continuous beam model is asymmetrically at the midpoint of the 2–3 segment, and the 1–2 and 3–4 segments rotate θ_3 clockwise and counterclockwise, respectively.

3.1.3. Elastic Foundation Beam Model

After all MRs are excavated and filled, the main roof is in contact with the filling body continuously. All the coal pillars are replaced by filling, resulting in the removal of stress isolation between continuous beams, and all spacing continuous beams are connected as a whole [37]. In order to establish the mechanical model of elastic foundation beam, the following assumptions are made: (1) the boundary of mining block imposes a constraint on the main roof, and there exists a supporting stress and bending moment on the filling body near the boundary to provide the main roof with a static balance. (2) When the main roof reaches a rebalancing state, the anchorage restraint of the connecting joints are relieved, and all points on the main roof are continuous and differentiable. (3) The strength of filling bodies meets the requirements of supporting and bearing, and there is no failure, so the pillar foundation bearing the main roof can be regarded as the elastic foundation. (4) The internal part of filling bodies can be transferred by interaction, and the elastic foundation can provide a uniformly-distributed support.

The mechanical model of beam on elastic foundation is shown in Figure 5d. Strata act on elastic foundation beam with uniformly distributed load q , and the filling bodies provide uniformly distributed support stress f . In this figure, the elastic foundation beam of 1–4 segment represents that the main roof has reached the rebalance state, the 5–6 segment represents that the basic roof is in the original rock stress state, and the 4–5 segment represents the transition stage from the original rock stress state to the rebalance state. Connecting joints 1, 2, and 3 represent the joints after removing the fixed support and constraints, which only provide support to the elastic foundation beam and no longer transfer the bending moment. Connecting joint 4 represents the critical point of the elastic foundation beam reaching the rebalancing state. Connecting joint 5 represents the boundary of the CECB working face, which is the fixed support end. Connecting joint 6 represents the original rock stress state.

3.2. Deformation Characteristics of the Beam Models

Based on the above analysis, taking the main roof as an example, the deformation characteristics of strata after each mining phase are studied.

3.2.1. The Structure of the Continuous Beam

After the third mining phase, the static equilibrium equation of the beam structure in the main roof can be written as:

$$M_{13} + \frac{(q-f)L_0^2}{2} - M_{23} - N_1L_0 = 0 \quad (1)$$

$$M_{23} + \frac{(q-f)L_0^2}{2} - M_{13} - F_1L_0 = 0 \quad (2)$$

$$3L_0(q-f) = F_1 + N_1 + 2N_2 + N_3 + F_4 \quad (3)$$

The maximum bending moment of the main roof at the connecting joints can be acquired and, therefore, the bending moments at different connecting joints can be calculated as:

$$\begin{cases} M_{13} = M_{43} = \frac{-(q-f)L_0^3 - 48E\theta_3 I_0}{12L_0} \\ M_{23} = M_{33} = \frac{-(q-f)L_0^3 + 24E\theta_3 I_0}{12L_0} \end{cases} \quad (4)$$

where F_i and N_i , the supporting force and the supporting force components at the i -th connecting joint ($i = 1, 2, \dots, 5$), respectively, kN; M_{ij} , the bending moments at the i -th connecting joint at the j -th phase ($i = 1, 2, \dots, 5; j = 1, 2, 3, 4$), kN·m; I_0 , the inertia moment of the main roof, m^4 ; L_0 , the width of the MR, m; f , the supporting force of the filling body, MPa; q , the load on the strata, MPa; θ_j , the inclination angle of the beam at the j -th phase ($j = 1, 2, 3, 4$), °; and E , the elastic modulus of the main roof, GPa.

The conditions at the third mining phase are evolved from those at the first two mining phases. The bending moment equations at the first two mining phases can thus be derived according to Equation (4) [17]. The bending moments at each connecting joint after the completion of the first two mining phases can be written as:

$$M_{11} = M_{21} = \frac{-(q-f)L_0^2}{12} \quad (5)$$

$$\begin{cases} M_{12} = M_{32} = \frac{-(q-f)L_0^3 - 48E\theta_2 I_0}{12L_0} \\ M_{22} = \frac{-(q-f)L_0^3 + 24E\theta_2 I_0}{12L_0} \end{cases} \quad (6)$$

3.2.2. The Structure of the Elastic Foundation Beam

Based on Winkler elastic foundation beam theories, the supporting strength of the bearing filling bodies in the main roof can be calculated as:

$$f(x) = kw(x) \quad (7)$$

where $w(x)$ is the subsidence of the main roof, and m and k are the foundation coefficients.

The subsidence of the main roof, the load in the strata, and the supporting strength of the filling bodies satisfy the following relation:

$$EI_0 \frac{d^4 w(x)}{dx^4} = q - f(x) \quad (8)$$

As shown in Figure 4d, the initial subsidence of the main roof, denoted as h_0 (with a unit of m) can be calculated as:

$$h_0 = L_0 \tan \theta_4 - x \tan \theta_4 \quad (9)$$

where x is the distance between the sinking position and coal wall, m.

By setting the characteristic coefficient $\beta = \sqrt[4]{\frac{k}{4EI_0}}$, the bending moment of the main roof can be written as:

$$M(x) = 2EI_0\beta^2 \left[e^{\beta x} (-A \cos \beta x + B \sin \beta x) + e^{-\beta x} (C \cos \beta x - D \sin \beta x) \right] \quad (10)$$

where A , B , C and D are coefficients to be determined.

The boundary conditions can be described as:

$$\begin{cases} w(0) = L_0 \tan \theta_4 \\ \frac{dw(0)}{dx} = 0 \end{cases} \quad \begin{cases} w(L_0) = 0 \\ \frac{dw(L_0)}{dx} = 0 \end{cases} \quad (11)$$

$e^{-\beta L_0}$ is approximate to 0. Accordingly, the approximate solutions of A, B, C, and D can be calculated as:

$$A = -\frac{\sin \beta L_0 + 4e^{\beta L_0} \sin 2\beta L_0 - e^{2\beta L_0} \cos \beta L_0}{3e^{\beta L_0} [1 - \sin 2\beta L_0 (e^{\beta L_0} + 1)]} \cdot \frac{\tan \theta_4}{\beta} + \frac{L_0 \tan \theta_4 (\cos^2 \beta L_0 + 5 \sin \beta L_0 \cos \beta L_0 + 3e^{2\beta L_0} \sin 2\beta L_0 - 3)}{3e^{\beta L_0} \sin \beta L_0 [1 - \sin 2\beta L_0 (e^{\beta L_0} + 1)]} + \frac{e^{2\beta L_0} \cos \beta L_0 (1 - 3 \sin 2\beta L_0) + \cos \beta L_0 (4 \sin^2 \beta L_0 - 2 \sin 2\beta L_0 + 3) + 2 \sin \beta L_0}{3e^{\beta L_0} \sin \beta L_0 [1 - \sin 2\beta L_0 (e^{\beta L_0} + 1)]} \cdot \frac{q}{k} \tag{12}$$

$$B = -\frac{2 \sin^2 \beta L_0 - e^{\beta L_0} \sin \beta L_0}{3[1 - \sin 2\beta L_0 (e^{\beta L_0} + 1)]} \cdot \frac{\tan \theta_4}{\beta} + \frac{e^{2\beta L_0} - 4 \sin^2 \beta L_0 - \sin 2\beta L_0 (3e^{2\beta L_0} + 4) - 2}{3[1 - \sin 2\beta L_0 (e^{\beta L_0} + 1)]} \cdot \frac{q}{k} \tag{13}$$

$$C = \frac{4e^{\beta L_0} \sin^2 \beta L_0 + 2e^{2\beta L_0} \sin \beta L_0 - 2 \sin \beta L_0 + e^{\beta L_0} \cos \beta L_0 (e^{\beta L_0} + 2)}{3e^{\beta L_0} (1 - e^{2\beta L_0} \sin 2\beta L_0)} \cdot \frac{\tan \theta_4}{\beta} + \frac{e^{\beta L_0} \sin \beta L_0 (6 \sin^2 \beta L_0 - 2e^{2\beta L_0} - e^{\beta L_0} \sin \beta L_0 \cos \beta L_0) + e^{\beta L_0} \cos \beta L_0 (\cos^2 \beta L_0 - e^{2\beta L_0} - 1)}{3e^{\beta L_0} \sin \beta L_0 (1 - e^{2\beta L_0} \sin 2\beta L_0)} \cdot \frac{q}{k} + \frac{L_0 \tan \theta_4 (2 \sin^2 \beta L_0 - \sin \beta L_0 \cos \beta L_0 - \cos^2 \beta L_0)}{3e^{\beta L_0} \sin \beta L_0 (1 - e^{2\beta L_0} \sin 2\beta L_0)} \tag{14}$$

$$D = \frac{2 \sin^2 \beta L_0 + e^{\beta L_0} \sin \beta L_0}{3 - 3 \sin 2\beta L_0 (e^{2\beta L_0} + 1)} \cdot \frac{\tan \theta_4}{\beta} + \frac{4 \sin^2 \beta L_0 - e^{2\beta L_0} - \sin 2\beta L_0 - 1}{3 - 3 \sin 2\beta L_0 (e^{2\beta L_0} + 1)} \cdot \frac{q}{k} \tag{15}$$

After the fourth mining phase, the maximum bending moment of the main roof can be calculated as:

$$M_{44} = M_{54} = 2EI_0\beta^2(A - C) \tag{16}$$

3.3. Fractures in the Overlying Strata

The critical condition for the generation of fractures in the overlying strata is that the tensile strain produced in bending deflection of the strata reaches the ultimate strain. Assuming that fractures in the strata develop towards the n -th stratum above the coal seam, a unit with a length of dx and a length of $2y$ was selected on the edge of fracture development. The distances between the upper/lower boundary of the unit and the neutral axis $O-O$ are denoted as y . As shown in Figure 6, during the deformation of left and right cross-sections, the unit is rotated by $d\varphi$ around the $P-P$ axis, with a curvature of ρ .

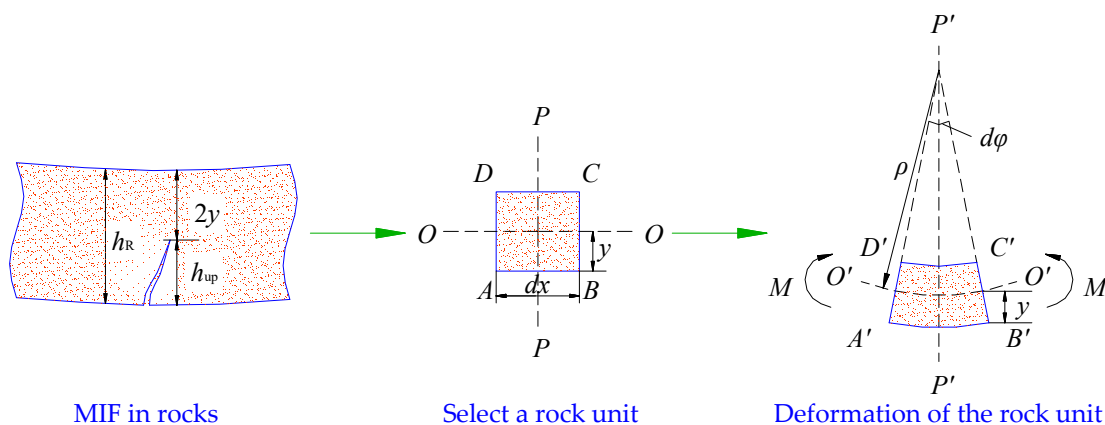


Figure 6. Volumetric strain analysis of rock element.

Under critical conditions, the strain of the side AB of the unit in the stratum can be calculated as:

$$\varepsilon_{AB} = \frac{(\rho + y)d\varphi - \rho d\varphi}{\rho d\varphi} \tag{17}$$

The ultimate strain (ε_m) of the stratum can be calculated as:

$$\varepsilon_m = \frac{12M_{ij} - \gamma h_{up} L_0^2}{2h_R^2 E} \quad (18)$$

where h_R is the thickness of the n -th stratum, m; γ is the unit weight of the n -th stratum, kN/m^3 ; and h_{up} is the development height of the fractures in the n -th stratum, m.

The subsidence of the stratum, the length of beam and the radius of curvature satisfy the following geometrical relation:

$$(\rho + h_{up} - w)^2 + L_0^2 = (\rho + h_{up})^2 \quad (19)$$

where w , the subsidence of the stratum, m, L_0 , the beam length, m, ρ , of the curvature radius, rad.

It can be calculated from the above that:

$$h_{up} = \frac{4wM_{ij} + \gamma L_0^4 - 2wh_R^2 E + \sqrt{(4wM_{ij} + \gamma L_0^4 - 2wh_R^2 E)^2 - 16w\gamma L_0(6M_{ij}L_0^2 - wh_R^3 E)}}{1.2\gamma L_0} \quad (20)$$

Accordingly, the MIF height is denoted as H_{up} (with a unit of m) in the stratum can be calculated as:

$$H_{up} = h_{up} + \sum_{i=0}^{n-1} h_i \quad (21)$$

where h_i denote the thickness of the i -th stratum above the coal seam ($i = 1, 2, 3 \dots$), m.

The MR filling percentage is the ratio of the volume of fully compacted filling bodies to the volume of coal mined out, which expressed in η . It is one of the key factors controlling the development of MIF. From Equation (21), the relationship between the MIF height and the MR filling percentage can be expressed in the form of hyperbolic function. Definition coefficient λ is used to characterize the influence of MR filling percentages on MIF. The relationship between H_{up} and η can be expressed as:

$$H_{up}^2 - [M(1 - \eta) + \lambda]^2 + \lambda^2 = 0 \quad (22)$$

where M is the thickness of the coal seam, m.

4. Characteristics of MIF

4.1. The Numerical Model and the Scheme

The universal distinct element code (UDCE) produced by Itasca Consulting Group, Inc. (Minneapolis, MN, USA) was used to analyze the characteristics of MIF under CECB. After rock failure, the parameters such as cohesion, internal friction angle, and tensile strength decrease rapidly with the increasing strain, which reflects strain-softening characteristics. However, the main characteristics of CECB include: (a) mining in the form of excavating the MRs, the exposed area of roof is smaller, and the deformation space of strata is minimized; (b) filling the MRs immediately after excavation to minimize the deformation time of strata; (c) interval excavated MRs can provide mutual lateral restraint between coal and filling to control the deformation of strata further. Although the parameters of fractured rock mass, such as cohesion are decreased, the reduction is limited in the conditions of confined deformation space and limited deformation time. In addition, CECB is put forward to solve the water conservation mining problems of low damage strata control. If there is a large deformation in the strata, this method will not be applicable. Based on the characteristics and suitable conditions of CECB, a Mohr–Coulomb model with a size of $300 \text{ m} \times 230 \text{ m}$ (length \times height) is established to study the characteristics of MIF. The width of mining area is 120 m and 90 m boundary pillars are left on both sides of the mining area. Displacement constraints are imposed on the left, right, and bottom

boundaries of the model. Surveying lines are laid at the top and bottom of each aquifer and each surveying line has 150 points, as shown in Figure 7. The parameter values of each stratum are shown in Tables 1 and 2 [24,25,38].

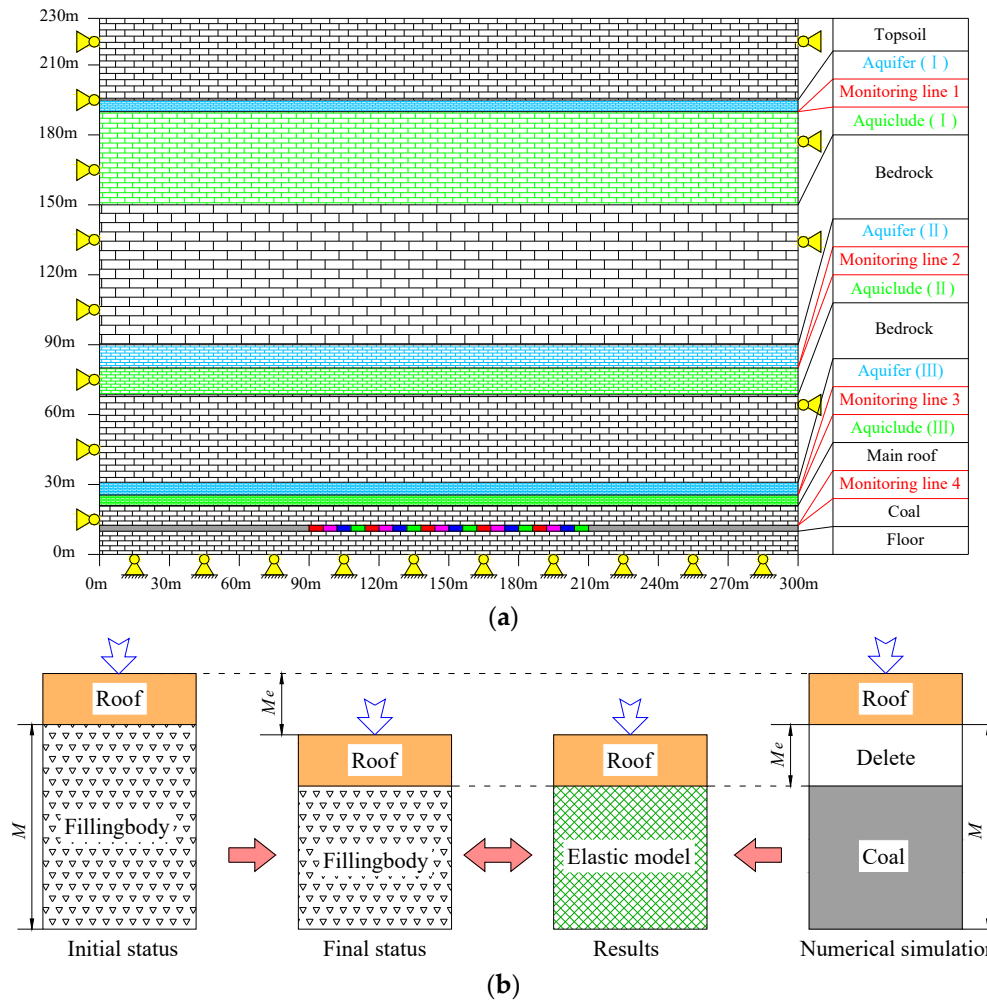


Figure 7. Numerical simulation models. (a) Diagram of model size, strata, and mining area; (b) the method of simulating the MR filling percentage.

Table 1. Rock physical and mechanical parameters (block).

Number	Stratum	Bulk Modulus (GPa)	Shear Modulus (GPa)	Density (kg/m ³)	Friction Angle (°)	Cohesion (MPa)	Tensile Strength (MPa)
1	Bauxitic mudstone	12.1	10.8	2450	19	1.0	1.0
2	Coal seam	3.9	2.3	1410	21	1.1	0.8
3	Limestone	21.9	18.2	2500	40	2.3	5.4
4	Mudstone	13.5	11.7	2350	23	1.0	1.0
5	Sandy mudstone	12.3	10.5	2400	22	1.0	1.0
6	Fine sandstone	31.2	20.9	2600	34	5.8	4.1
7	Medium sandstone	21.8	14.0	2550	30	4.3	2.2
8	Clay	8.5	4.2	2200	25	2.0	0.9

Table 2. Rock physical and mechanical parameters (contact).

Number	Strata	Normal Stiffness (GPa/m)	Shear Stiffness (GPa/m)	Cohesion (MPa)	Friction Angle (°)	Tensile Strength (MPa)
1	Bauxitic mudstone	1.1	0.8	0.5	12	0.3
2	Coal seam	4.0	2.0	0.3	15	0.5
3	Limestone	1.8	1.2	0.9	30	0.6
4	Mudstone	0.9	0.7	0.4	10	0.2
5	Sandy mudstone	1.0	0.8	0.5	10	0.3
6	Fine sandstone	0.8	0.6	0.6	13	0.5
7	Medium sandstone	0.7	0.5	0.5	14	0.4
8	Clay	0.3	0.1	0.2	18	0.1

The mining area is divided into four mining phases, and each mining phase contains 5 MRs, the size of which is 6 m (width) \times 2.5m (height). Equivalent mining height theories hold that filling materials occupy part of overburden subsidence space, which is equivalent to reducing mining height [39,40]. The MR filling percentage can be expressed as:

$$\eta = \frac{M - M_e}{M} \quad (23)$$

where M_e is equivalent to the mining height, m.

In the numerical calculation, the method of a deleting grid is used to realize the different MR filling percentages. We delete the height of M_e from top to bottom in the model of a coal seam, and set the rest as the elastic model. Then, we set enough elastic modulus in the elastic model to ensure that the deformation of elastic model is far less than M_e in the whole mining process, so as to realize CECB in different MR filling percentages. For example, a 90% MR filling percentage is achieved by deleting 10% from the height of the coal seam model in each mining phase from top to bottom. According to the above method, the characteristics of MIF in the excavating of MRs are calculated under the conditions of 10%, 20%, 30%, 40%, 50%, 60%, 70%, 80%, and 90 MR filling percentages respectively.

4.2. Distribution Patterns of MIF

4.2.1. The Elastic Foundation Beam Structure

The CECB can protect the main roof from breaking or caving by filling the excavated MR in time to reduce the development of MIF, and ultimately realize water conservation mining. Therefore, the higher the MR filling percentage is, the better the controlling effect of the MIF is, and the more advantageous to water conservation mining. Taking a 90% MR filling percentage as an example, the formation and evolution process of MIF under CECB is further studied. The “plot pen block open” command is used to display the distribution of MIF in each mining phase under CECB, as shown in Figure 8.

The first two mining phases have interval distribution of MIF. At the end of the first mining phase, MIF only exist above the mining area. The highest point of MIF is located in the middle of the mining area, and gradually decreases to both sides of the mining area, the shape of which is approximately triangular. MIF have discontinuous distribution because of the isolation of the coal pillars. At the end of the mining phase, MIF form a saddle shape with high sides and low middle sides over the mining area. Micro-cracks appear in aquiclude III and aquifer III. In this phase, MIF still have a discontinuous distribution.

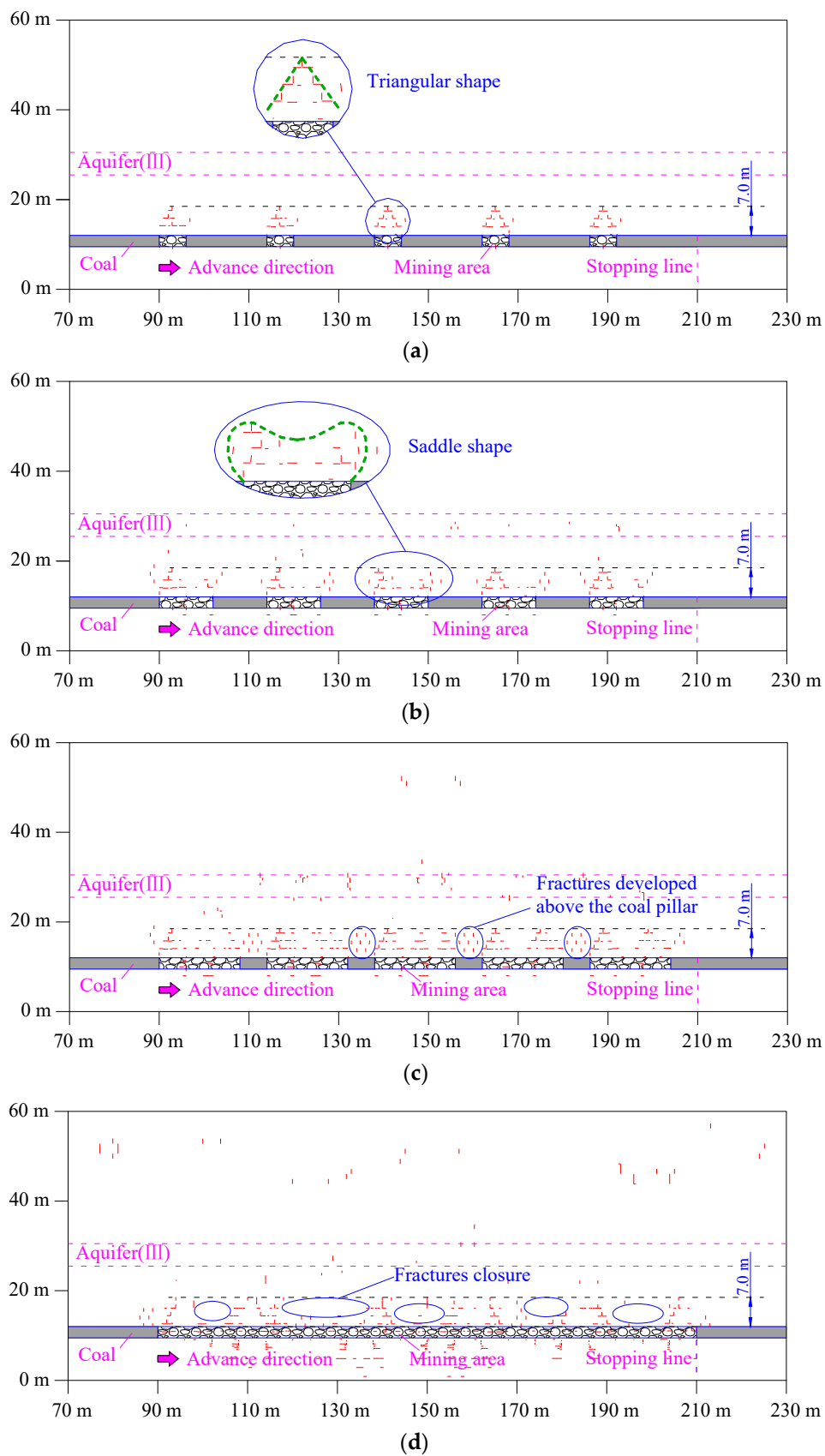


Figure 8. The distribution pattern of MIF in 90% MR filling percentage. (a) The 1st mining phase; (b) the 2nd mining phase; (c) the 3rd mining phase; (d) the 4th mining phase.

However, MIF in the last two mining phases are continuously distributed. At the end of the third phase, MIF are connected with each other, which include interlayer fractures formed by failure along the upper and lower surface of the grids and longitudinal fractures formed by failure along the left and right surfaces of the grids. Among them, there are only longitudinal fractures along the left and right surfaces of the grids above the coal pillar. This shows that the excavating MRs lead to the subsidence of overlying strata, and the asynchronism of the subsidence of each strata produces interlayer fractures, while the strata are also subjected to horizontal tensile stress to produce fractures. The strata above the coal pillar are mainly caused by horizontal tension stress and longitudinal fractures. At the end of the fourth phase, MIF are connected with each other, but the density of the fractures decreases compared with the third phase. After recovering the last part of the coal pillar, all the cushions bearing the main roof become the same kind of medium, and the main roof acts on the elastic foundation under a uniform force, and the horizontal tensile stress decreases. In the last phase, the longitudinal fractures are closed due to the horizontal tensile stress. During the whole CECB, the MIF height in each phase is almost unchanged, which is 7.0 m (2.8 times the mining height).

4.2.2. The Elastic Foundation Beam Structure

Figure 8 shows the distribution patterns of MIF after CECB. By comparing and analyzing the characteristics of MIF in different MR filling percentages, it can be concluded that the displacement angle of overlying strata is about 66 degrees, and this hardly changes by the changed MR filling percentages. Combining with Figures 8d and 9, when the filling percentage (of the mined voids) is not less than 30%, there is no obvious difference between the middle and the edge of the working face, which is approximately the same height. Therefore, unlike the saddle-shaped distribution pattern of traditional longwall mining, the MIF under CECB are approximately isosceles trapezoidal distribution.

In the conditions of different MR filling percentages, the distribution patterns of MIF are a group of isosceles trapezoids with the same bottom edge, the same inclination angle of two waists and different heights. The above analysis shows that the parameters such as fracture distribution pattern and displacement angle of overlying strata are not sensitive to the change of MR filling percentages. The MR filling percentage, however, is an important index affecting the MIF height.

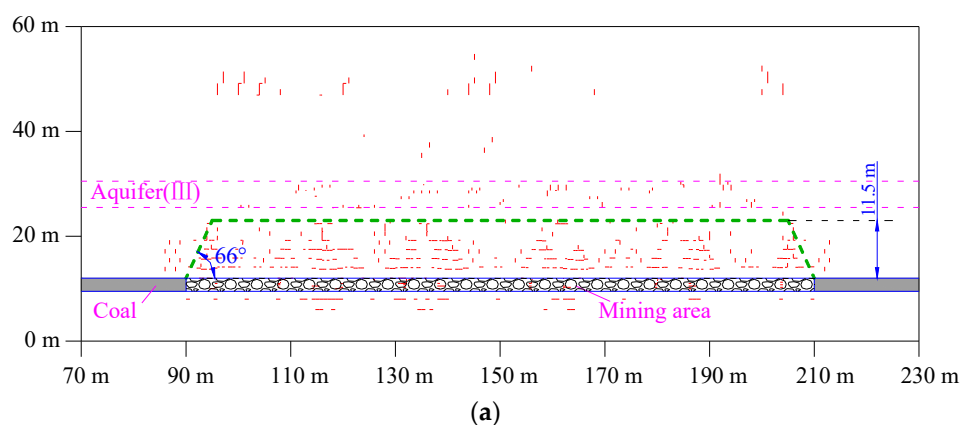
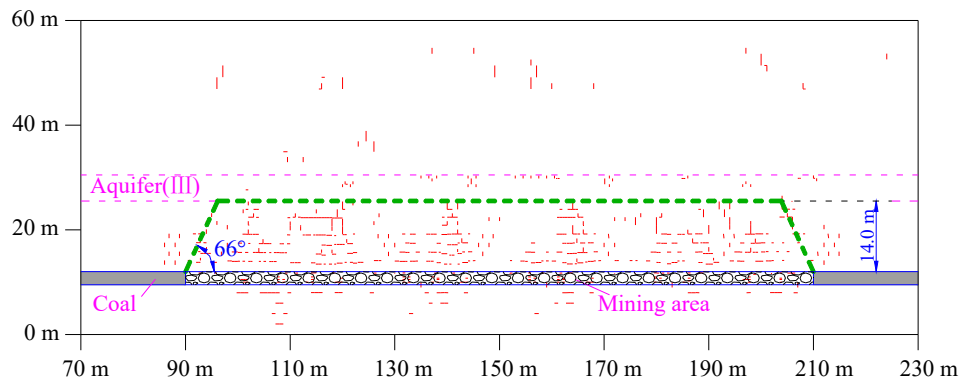
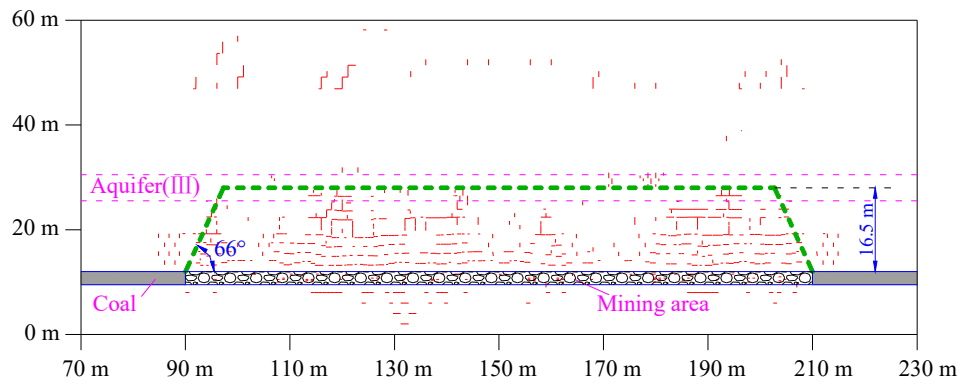


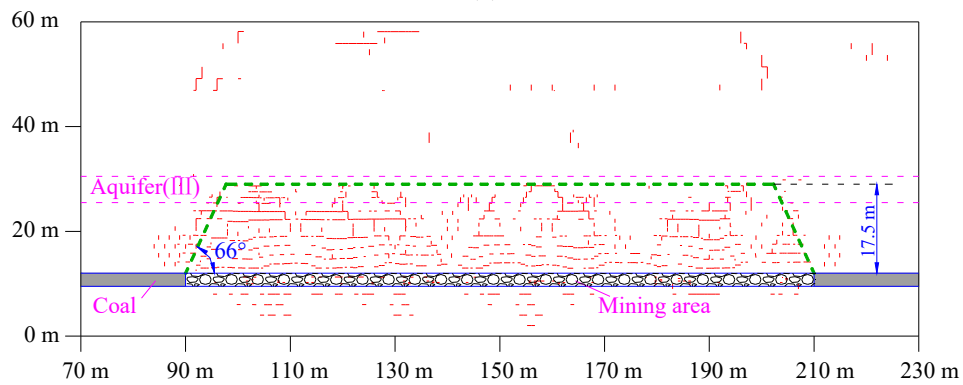
Figure 9. Cont.



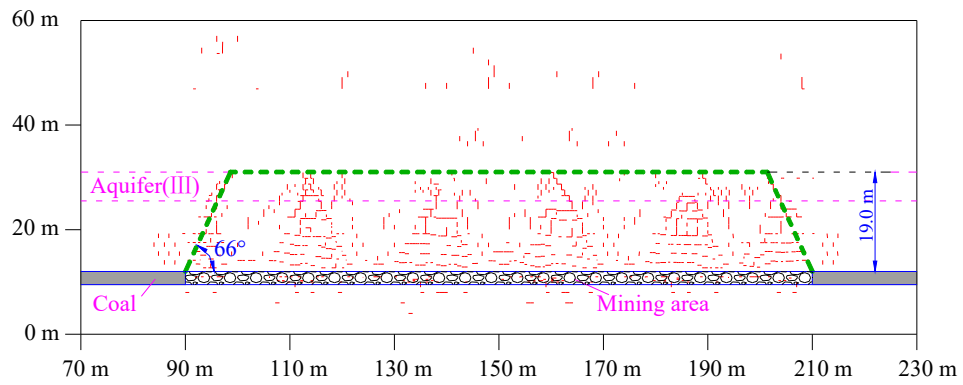
(b)



(c)



(d)



(e)

Figure 9. Cont.

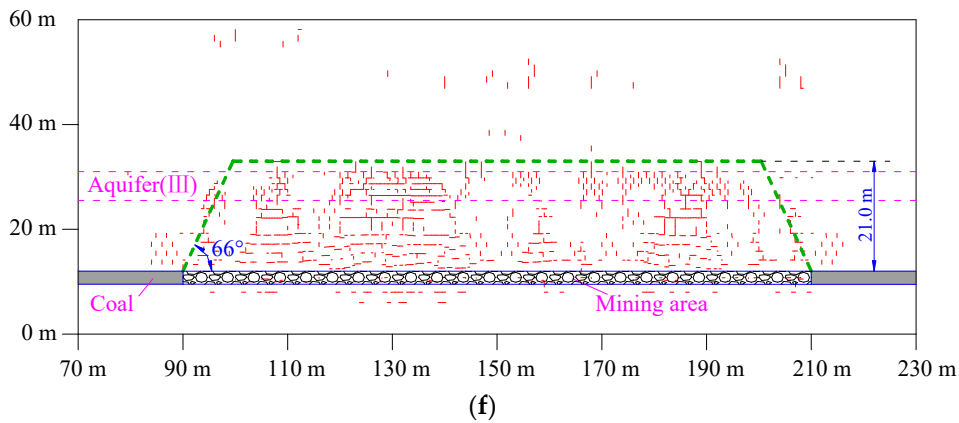


Figure 9. The distribution pattern of MIF in different MR filling percentages. (a) $\eta = 80\%$; (b) $\eta = 70\%$; (c) $\eta = 60\%$; (d) $\eta = 50\%$; (e) $\eta = 40\%$; (f) $\eta = 30\%$.

4.3. Influences of MR Filling Percentages on MIF

According to Equations (22) and (23), the effects of MR filling percentages on the MIF height can be expressed by two parameters: the influence of MR filling percentages on MIF (λ) and the ratio of the MIF height to equivalent mining height (μ). In order to display the movement of grids more intuitively, the numerical results are redisplayed by using “boundary plot” command. The curves of $H_{up}-\eta$, $\lambda-\eta$ and $\mu-\eta$ are plotted under different MR filling percentages, respectively, as shown in Figure 10.

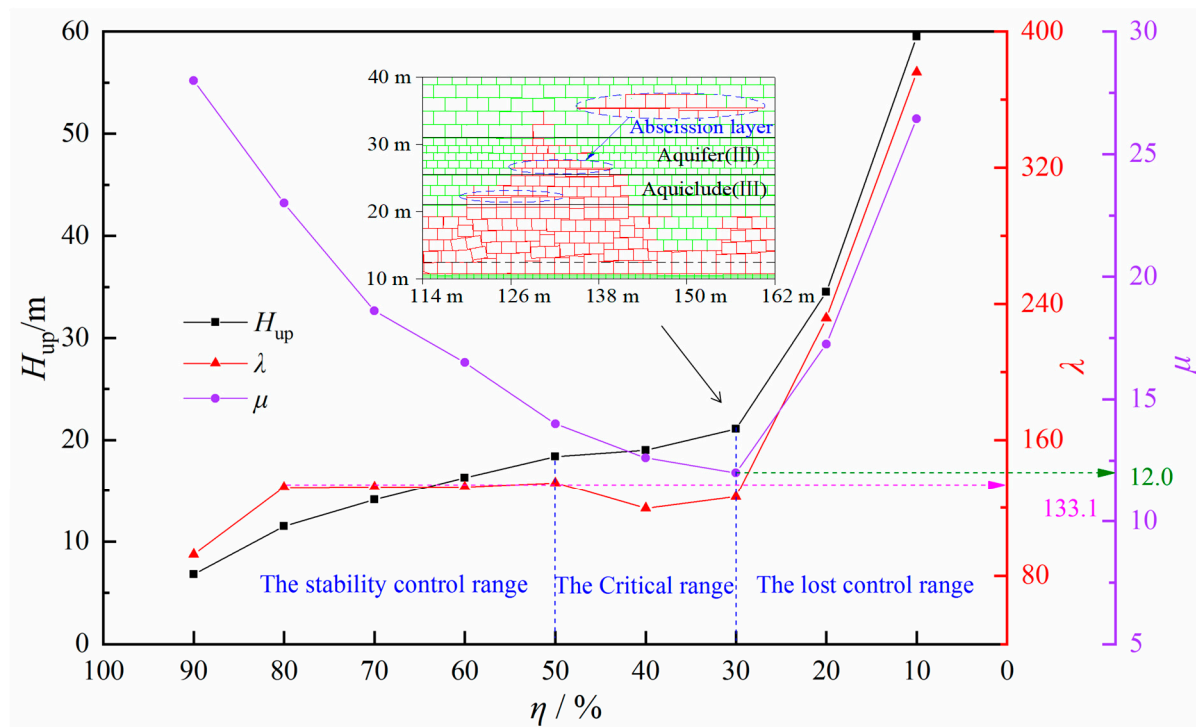


Figure 10. The control of MIF height under CECB.

When the MR filling percentage decreases from 90% to 30%, the growth rate of H_{up} is relatively slow, from 2.8 times to 8.4 times, and the value of λ keeps around 133.1. When the MR filling percentage decreases from 30% to 10%, H_{up} increases from 8.4 times to 23.8 times, and the value of λ increases from 126.3 to 376.1. Therefore, the MIF height (H_{up}) is correlated with λ . In addition, when the MR filling percentage decreases from 90% to 30%, the trend of the increasing height of MIF is slowed down and the value of μ gradually decreases. When the MR filling percentage is less than 30%, the MIF

height increases rapidly and the value of μ increases gradually. Therefore, the growth rate of the MIF height (ΔH_{up}) is correlated with μ . The comparison between $H_{up-\lambda}$ and $\Delta H_{up-\mu}$ in different MR filling percentages is shown in Table 3.

Table 3. The comparison table between $H_{up-\lambda}$ and $\Delta H_{up-\mu}$ in different percentages.

MR Filling Percentages	90%	80%	70%	60%	50%	40%	30%	20%	10%
H_{up}	7.0	11.5	14.1	16.3	18.4	19.0	21.1	30.5	49.5
μ	92.4	132.0	132.2	132.3	134.8	119.6	126.3	231.6	376.1
ΔH_{up}	7.0	4.7	2.6	2.2	2.1	0.6	2.1	13.4	25.0
μ	28.0	23.0	18.6	16.5	14.0	12.6	12.0	17.25	26.44

The Pearson correlation coefficients of $H_{up-\lambda}$ and $\Delta H_{up-\mu}$ are calculated using the following formula:

$$r(x, y) = \frac{Cov(x, y)}{\sqrt{Var(x)Var(y)}} \quad (24)$$

where $Cov(x, y)$, the covariance of two sets of data, x and y ; $Var(x)$, variance of data x ; and $Var(y)$, variance of data y . The calculated results show that the Pearson correlation coefficients of $H_{up-\lambda}$ and $\Delta H_{up-\mu}$ are 0.98 and 0.61, respectively, and the correlation grades are very strong and moderate, respectively.

By using parameter λ as the main index, the controlling effects of MR filling percentages on MIF can be described more accurately. The $H_{up-\eta}$ curve is divided into three ranges according to the change of H_{up} and λ in different MR filling percentages. They are the stability control range, the critical range and the lost control range. When the MR filling percentage is more than 50%, the MIF height increases steadily, and the overall stability of λ is maintained. Filling bodies can effectively support the strata, and the MIF height increases steadily with the decrease of the MR filling percentage, which reflects the stable control of the filling bodies on the development of MIF. When the MR filling percentage is between 30% and 50%, although the MIF height increases steadily, the amplitude of λ fluctuates and decreases. The gradual decrease of the MR filling percentage leads to the intensification of overlying strata migration, the separation between soft rock and hard rock, and the temporary slowing down the MIF development. Abscission layer is the sign of unstable state of overlying strata migration. Therefore, this range is the critical state of filling bodies' transition from stable control to lost control of MIF development. When the MR filling percentage is less than 30%, the MIF height increases sharply, which indicates the control of filling bodied is invalid.

According to the influence of MR filling percentages on MIF, the necessary condition for filling bodies to play a stable control role is that the MR filling percentage is not less than 50%. When the MR filling percentage is more than 50%, the MIF height can be expressed as follows:

$$H_{up} = \begin{cases} 1.58 \sqrt{82.5\eta^2 - 385\eta + 302.5} & (\eta \geq 85\%) \\ 1.58 \sqrt{-22.2\eta^2 - 269.7\eta + 268.7} & (85\% > \eta \geq 50\%) \end{cases} \quad (25)$$

5. Engineering Practices

5.1. Arrangement of MRs

In the study area using two wings to arrange MRs, which opens at 50 degrees on both sides of the head entry, and the width of the MR is 6 m. The MRs are divided into four mining phases. In the same mining phase, the width of the isolation structure is 18 m (that is, three MRs per interval). All the MRs are excavated in turn, and filling of the excavated MRs is done immediately. The operation mode of "parallel excavating and filling" is always maintained until the end of mining, as shown in Figure 11.

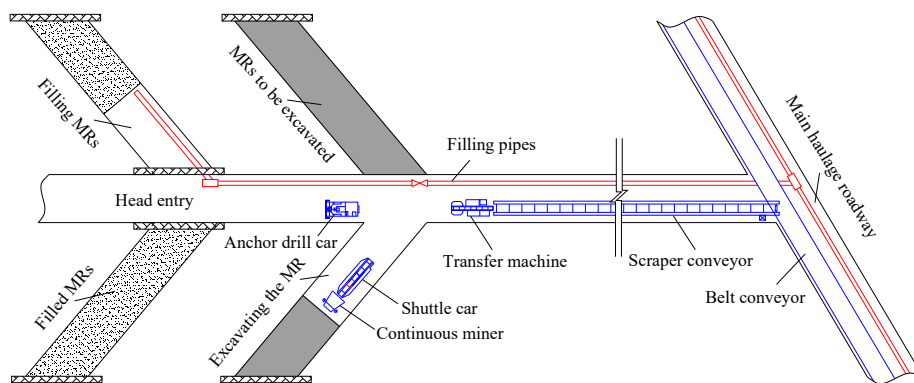


Figure 11. Schematic diagram of “parallel excavating and filling” operation mode.

5.2. The Critical MR Filling Percentage

The filling materials are high-water swelling materials. The aggregate is fly ash, and the auxiliary materials are lime, gypsum, cement, additives, etc. The filling material is mixed with water to make high-water swelling materials with a mass ratio of 1.40:1 and a density of 1.55 g/cm³, which is filled into the MRs. After 28-day solidification, the strength of filling body was approximately 5.0 MPa [25]. By using the condition of whether MIF cut through the aquiclude as the judgement criterion of the aquiclude failure, the critical MR filling percentage for achieving water conservation mining in the study area is determined as 83.2%.

5.3. Effects of Water Conservation

By taking into account safety coefficient and construction factors, the MR filling percentage was set as 90%. The theoretical calculation result of the MIF height is 7.55 m (3.0 times mining height) and the numerical results is 7.0m (2.8 times mining height). The above two methods calculate results that the MIF height are less than the main roof thickness, so MIF do not penetrate the main roof. However, affected by mining, water resources in aquifer III might still be lost.

In order to study the influence of water level in aquifer above MIF under the condition of CECB, a fluid-mechanical coupling model using FLAC3D was established. The size of CECB working face is 330 m × 210 m (strike × dip), and the distance between the working face and the model boundary is considered to be no less than 1.2 times of coal seam buried depth. The physical and mechanical parameters of each strata are consistent with those in Table 1. The size of the fluid–mechanical coupling model is determined as 900 m × 800 m × 230 m (length × width × height), as shown in Figure 12.

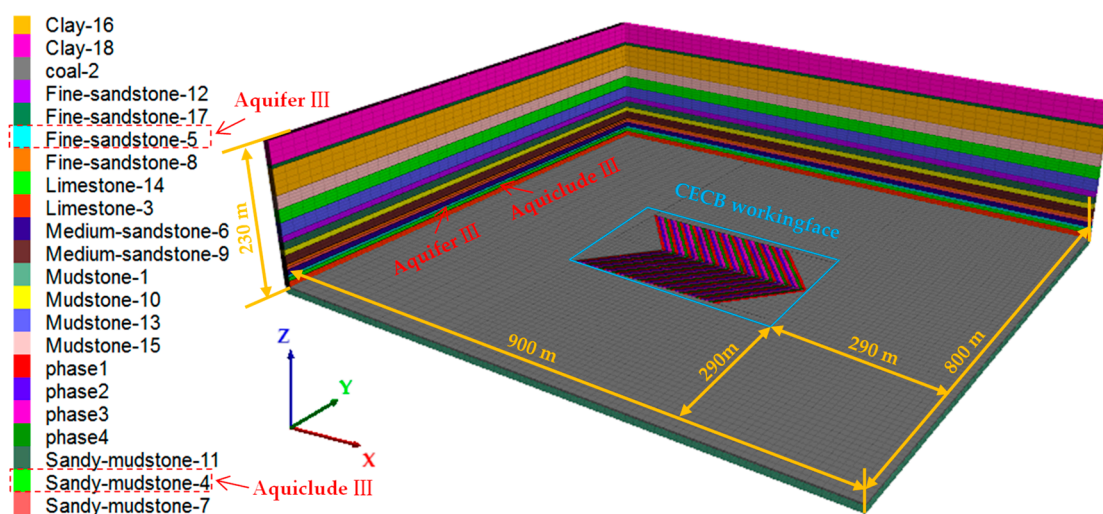


Figure 12. The numerical fluid–mechanical coupling model under CECB.

At the beginning of numerical calculation, use the code “CONFIG Fluid” to set the seepage calculation mode. The Mohr–Coulomb model is the same as the previous one. We set the water level in aquifer III, and the vertical distance to the bottom boundary of aquifer III is 3 m. The initial value and pore pressure gradient in the code “INITIAL pp” can be calculated. The default porosity of FLAC3D is 0.5. In the fluid–mechanical coupling model, the porosities of limestone and other hard rocks are slightly higher than that of mudstone and other soft rocks. In order to achieve the calculated equilibrium state, the porosities are not less than 0.2. It is divided into four phases to excavate and fill the MRs, and calculate the pore pressure in the strata. After data processing, the contour map of water level drawdown in aquifer III is obtained (Figure 13).

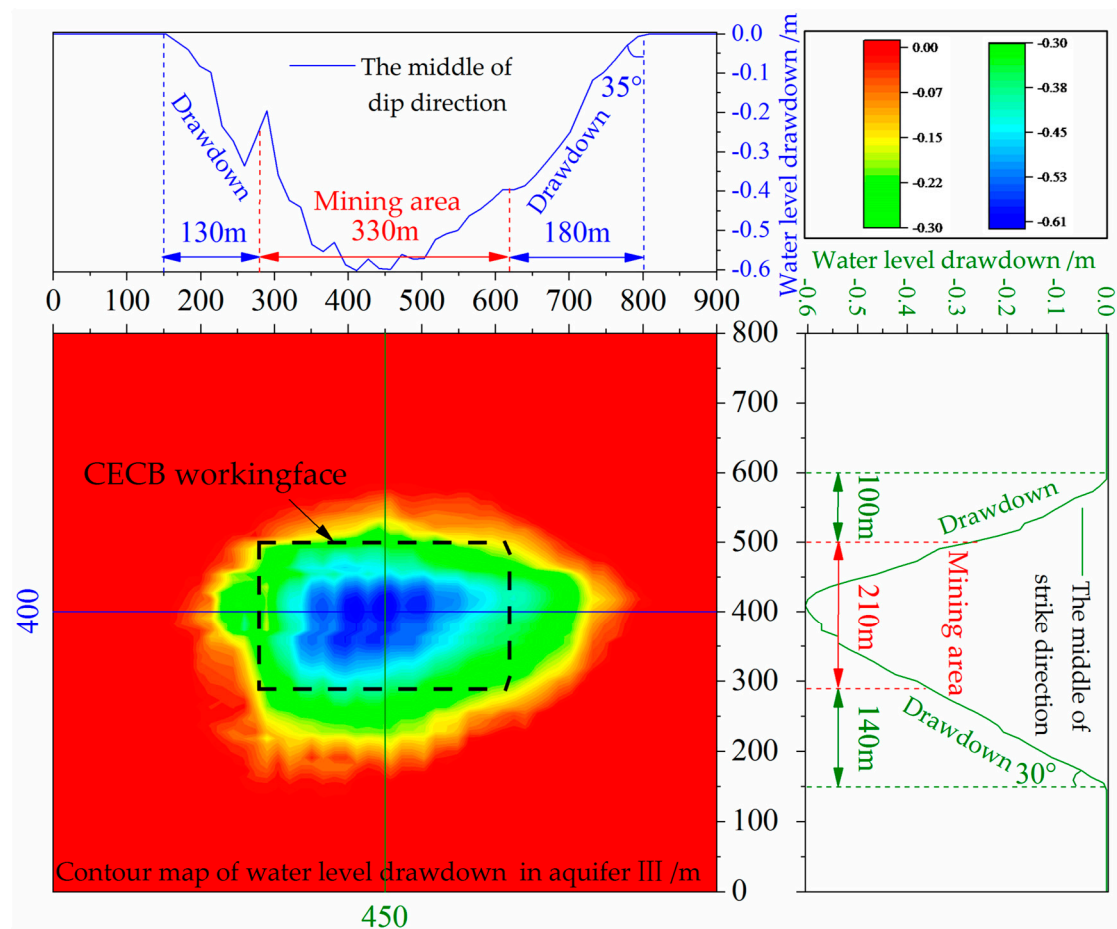


Figure 13. The contour map of water level drawdown in the study area after CECB.

It is determined that the maximum drawdown of aquifer III is 0.61 m, which occurs in the middle of CECB working face. The section lines are made along the middle strike and dip of the working face. The result is that on both sides of the strike direction of CECB working face, the range of water level drawdown is 130 m and 180 m, respectively, and on both sides of the dip direction, the range of water level drawdown is 100 m and 140 m, respectively. Considering the maximum influence range, the average recovery of water level is 3.39×10^{-3} m along the strike direction for every 1m away from CECB working face, and 4.36×10^{-3} m along the dip direction. Although the water level in the vicinity of the mining area is decreased due to mining activities, the water resources in aquifer III did not completely leak. As the distance to the CECB working face increases, the water level gradually returns to the initial state. It is considered that aquiclude III is not destroyed, and water conservation mining is realized in the study area [41,42].

6. Discussions

(1) Advantages of CECB

The background of CECB is to solve the limitation of traditional longwall backfilling mining, which concludes:

(a) the exposed area of the roof in longwall mining is larger, and the overburden migration is relatively significant, which is not conducive to the support of the roof by the filling body; (b) the filling body is lack of lateral constraints after filling into the goaf, and its deformation resistance is weak; and (c) the mining activities and filling operations are mutually constrained, which not only affects the mining efficiency, but is difficult to ensure the full compaction of backfill.

The advantages of CECB are as follows:

(a) mining in the form of excavating MRs, the exposed roof area is smaller than longwall mining, and the roof is supported by coal pillars or filling bodies on both sides of MRs, so as to minimize the migration degree of overburden; (b) the filling body is filled into the confined space, which is always in the state of three-dimensional stress, and its deformation is relatively small; (c) the mining activities and filling operations are independent in space and do not interfere with each other, so the efficiency of mining and filling is high; and (d) both sides of the MRs just filled are not excavated immediately, which provide sufficient time and effective space for the solidification and full bearing of the filling body.

(2) Comparison the results by using strain-softening model and Mohr–Coulomb model

To check the feasibility by using Mohr–Coulomb model and rationality of the numerical results, a strain-softening model with 90% MR filling percentage is established and studied. The general parameters of each stratum are the same as those in Mohr–Coulomb model, such as bulk modulus, shear modulus, density, internal friction angle, cohesion, and tensile strength. Then the additional parameters, such as c_{table} , f_{table} , and t_{table} , are determined by the plastic zone characteristics of the total stress–strain curves through uniaxial compression tests. The numerical results are shown in Figure 14.

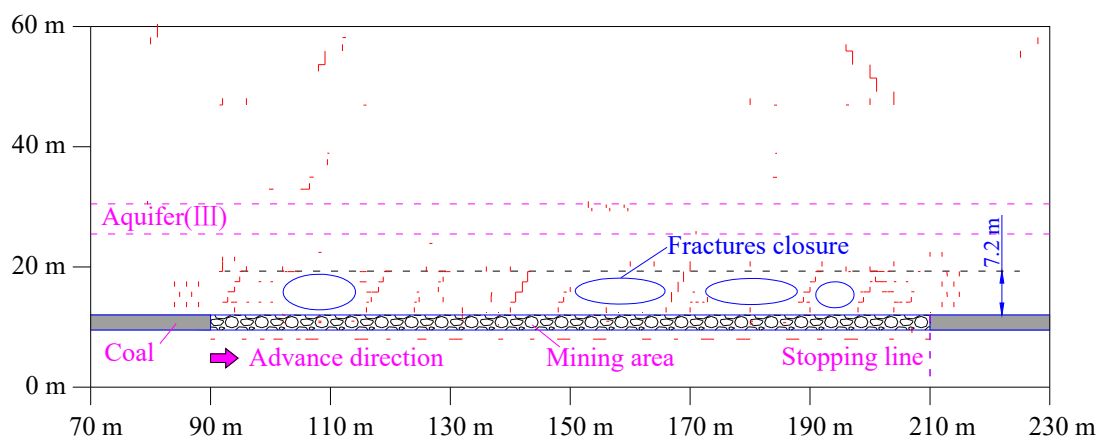


Figure 14. The distribution of MIF in 90% MR filling percentage by using the strain-softening model.

It is determined that the density and the range of MIF obtained by the Mohr–Coulomb model and strain-softening model are similar. In strain-softening model, the height of MIF is 7.2 m (2.88 times the mining height), which is slightly higher than the 7.0 m (2.8 times of mining height) calculated by using Mohr–Coulomb model. The differences between the two results are about 3%, but both are smaller than the theoretical calculation value. Therefore, it is also feasible to use the Mohr–Coulomb model to study the characteristics of MIF under CECB. In addition, the numerical results of the two models are smaller than the theoretical results. From the perspective of water conservation mining, the height of

MIF is predicted by the theoretical calculation value, which can also avoid the influence caused by the selection of different numerical models.

(3) Selection of mining and filling parameters

The influence of MR filling percentages on MIF is affected by factors, such as mining technology, backfilling technology, and geometrical conditions. The influencing factors mainly include the strength of the backfilling materials, the MR filling percentage, the MR height-to-width ratio, and the interval MR width. This study performed single-variable analysis for examining the effect of the filling percentage on the MIF height, during which the effects of other factors were not taken into account.

A smaller MR height-to-width ratio, more mining phases, and slighter roof subsidence can contribute to controlling the MIF height, but simultaneously reduce the mining efficiency. Higher strength of the filling materials and higher MR filling percentages can more remarkably control the MIF height; however, the utilization rate of the backfilling materials dropped. A reasonable arrangement of the MR and setting of backfilling parameters can not only achieve the function of water conservation mining in extremely close distance aquifers, but can also ensure the effectiveness of mining and increase the utilization rate of materials.

(4) Methods of improving coal mining efficiency

In actual production, the MR filling percentage is generally greater than that of excavation. In order to achieve coordinated operation of mining and filling, parallel excavation of multiple MRs can be carried out, which is similar to the simultaneous cutting of multiple shearers in the same working face. On the premise of meeting the requirement of water conservation mining, filling materials are not limited to one kind. High water expansion materials, aeolian sand paste-like materials, and industrial solid waste can be selected.

(5) Advantages of promotion

Filling cost is an important issue affecting the promotion and application of CECB. One advantage of this method is that the filling of MR can be adapted to local conditions and the comprehensive benefits of coal mining can be maximized. For example, in the northwest mining area of China, filling materials are difficult to obtain in situ materials. On the premise of water conservation mining, the filling quantity of MRs can be reduced appropriately, so as to reduce the filling cost. In the eastern mining area of China, the filling materials of industrial solid waste residue mainly consisting of gangue are sufficient and cheap, and MRs can be fully filled, which not only realizes the water conservation mining in the conditions of extremely close distance aquifers, but also solves the pollution problem of industrial solid waste residue to the surface environment.

(6) Scientific and social significance

The scientific significance of this study lies in providing theoretical guidance for water conservation mining under the extremely thin barrier layers, including mining under the extremely close-distance aquifers, mining close-distance coal seams, and other geological conditions. At present, CECB has been widely used in Ordos, Jincheng, Xinwen, and Zaozhuang mining areas in China. On the premise of water conservation mining, more than 2.6 million tons of recovered coal has been increased in total in the above mining areas, which increased profits by more than 67 million dollars, and achieved good economic and environmental benefits. With a view of realizing efficient, safe, and green mining of coal resources, CECB will be gradually extended to the core coal production bases in Western China.

7. Conclusions

According to the different boundary conditions of gradual replacement of the main roof stress from coal pillars to filling bodies, the mechanical models of clamped-clamped beam, continuous beam, and elastic foundation beam are established. The horizontal tensile strains of the overlying

strata are calculated, and the relationship between the MIF height and MR filling percentages satisfy a hyperbolic function.

The distribution patterns of MIF under CECB are studied. It is concluded that the distribution pattern is an isosceles trapezoid with the moving angle of the overlying strata as the bottom angle, and the upper and lower boundary of MIF as two parallel sides. Furthermore, the moving angle of the overlying strata does not change with MR filling percentages.

The controlling effects of MR filling percentages on MIF are studied. Taking the value of λ as the main index, the curve of the MIF height is divided into three ranges, including the stability control range, the critical range, and the lost control range. In addition, the calculating expression of the MIF height in the stability control range is given.

In the study area, the 90% MR filling percentage is used for CECB. The MIF height is 7.55 m (3.0 times mining height), and the main roof is not penetrated. The aquiclude III is effectively protected by the main roof, and its water-resisting property is not destroyed, thus realizing water conservation mining.

Author Contributions: S.W. conceived the research and wrote the paper. L.M. revised and reviewed the manuscript. All authors have read and approved the final manuscript.

Funding: This research was funded by National Key Basic Research Program of China (973 Program) grant number 2015CB251600, National Natural Science Foundation of China grant number 51874280 and the Priority Academic Program Development of Jiangsu Higher Education Institutions grant number PAPD.

Conflicts of Interest: The authors declare that they have no competing financial interests in connection with the work submitted.

References

- Xie, H.P.; Wu, L.X.; Zheng, D.Z. Prediction on the energy consumption and coal demand of China in 2025. *J. China Coal Soc.* **2019**, *44*, 1949–1960.
- Fan, L.M. Scientific connotation of water-preserved mining. *J. China Coal Soc.* **2017**, *42*, 27–35.
- Howladar, M.F. Coal mining impacts on water environs around the barapukuria coal mining; area, dinajpur, Bangladesh. *Environ. Earth Sci.* **2013**, *70*, 215–226. [[CrossRef](#)]
- Zhang, D.S.; Li, W.P.; Lai, X.P.; Fan, G.W.; Liu, W.Q. Development on basic theory of water protection during coal mining in northwest of China. *J. China Coal Soc.* **2017**, *42*, 36–43.
- Ma, L.Q.; Sun, H.; Wang, F.; Liang, J.M.; Jin, Z.Y.; Zhang, W. Analysis of the ground water level change of aquifer-protective mining in longwall coalface for shallow seam. *J. Min. Saf. Eng.* **2014**, *31*, 232–235.
- Yang, D.J.; Bian, Z.F.; Lei, S.G. Impact on soil physical qualities by the subsidence of coal mining: A case study in western china. *Environ. Earth Sci.* **2016**, *75*, 652.
- Azapagic, A. Developing a framework for sustainable development indicators for the mining and minerals industry. *J. Clean. Prod.* **2004**, *12*, 639–662. [[CrossRef](#)]
- Ma, D.; Miao, X.X.; Bai, H.B.; Huang, J.H.; Pu, H.; Wu, Y.; Zhang, G.M.; Li, J.W. Effect of mining on shear sidewall groundwater inrush hazard caused by seepage instability of the penetrated karst collapse pillar. *Nat. Hazards* **2016**, *82*, 73–93. [[CrossRef](#)]
- Gomes, C.J.B.; Costa, J.F.C.L. The environmental impact of coal mining: A case study in Brazil's sangão watershed. *Mine Water Environ.* **2011**, *30*, 159–168. [[CrossRef](#)]
- Galhardi, J.A.; Bonotto, D.M. Hydrogeochemical features of surface water and groundwater contaminated with acid mine drainage (amd) in coal mining areas: A case study in southern Brazil. *Environ. Sci. Pollut. Res.* **2016**, *23*, 1–17. [[CrossRef](#)]
- Mather, J.D.; Gray, D.A.; Jenkins, D.G. The use of tracers to investigate the relationship between mining subsidence and groundwater occurrence at aberfan, south wales. *J. Hydrol.* **1969**, *9*, 136–154. [[CrossRef](#)]
- Fawcett, R.J.; Hibberd, S.; Singh, R.N. An appraisal of mathematical models to predict water inflows into underground coal workings. *Int. J. Mine Water* **1984**, *3*, 33–54. [[CrossRef](#)]
- Booth, C.J. Strata-movement concepts and the hydrogeological impact of underground coal mining. *Ground Water* **2010**, *24*, 507–515. [[CrossRef](#)]

14. Li, W.P.; Ye, G.J.; Zhang, C.; Duan, Z.H.; Zhai, L.J. Study on the engineering geological conditions of protected water resources during coal mining action in Yu-Shen-Fu Mine Area in the North Shanxi Province. *J. China Coal Soc.* **2000**, *25*, 449–454.
15. Miao, X.X.; Pu, H.; Bai, H.B. Principle of Water-Resisting Key Strata and Its Application in Water-Preserved Mining. *J. China Univ. Min. Technol.* **2008**, *37*, 1–4.
16. Ma, L.Q.; Jin, Z.Y.; Liang, J.M.; Sun, H.; Zhang, D.S.; Li, P. Simulation of water resource loss in short-distance coal seams disturbed by repeated mining. *Environ. Earth Sci.* **2015**, *74*, 5653–5662. [[CrossRef](#)]
17. Sun, Q.; Zhang, J.X.; Zhou, N. Study and discussion of short-strip coal pillar recovery with cemented paste backfill. *Int. J. Rock Mech. Min. Sci.* **2018**, *104*, 147–155. [[CrossRef](#)]
18. Sheshpari, M. A review of underground mine backfilling methods with emphasis on cemented paste backfill. *Electron. J. Geotech. Eng.* **2015**, *20*, 5183–5208.
19. Jiang, H.Q.; Miao, X.X.; Zhang, J.X.; Liu, S.W. Gateside packwall design in solid backfill mining—A case study. *Int. J. Min. Sci. Technol.* **2016**, *26*, 261–265. [[CrossRef](#)]
20. Martin, J.; Holger, W. Progress in the research and application of coal mining with stowing. *Int. J. Min. Sci. Technol.* **2013**, *23*, 7–12.
21. Tan, Y.; Guo, W.B.; Bai, E.H.; Yang, D.M.; Xu, G.S.; Yan, H. Overburden failure induced by instability of coal pillar in strip Wongawilli mining. *J. China Coal Soc.* **2017**, *42*, 1656–1662.
22. Guo, W.B.; Xu, F.Y. Numerical simulation of overburden and surface movements for Wongawilli strip pillar mining. *Int. J. Min. Sci. Technol.* **2016**, *26*, 71–76. [[CrossRef](#)]
23. Zhang, J.X.; Sun, Q.; Zhou, N.; Jiang, H.Q.; Germain, D.; Abro, S. Research and application of roadway backfill coal mining technology in western coal mining area. *Arab. J. Geosci.* **2016**, *9*, 558. [[CrossRef](#)]
24. Ma, L.Q.; Zhang, D.S.; Wang, S.K.; Xie, Y.S.; Yu, Y.H. Water-preserved mining with the method named “backfilling while mining”. *J. China Coal Soc.* **2018**, *43*, 62–69.
25. Wang, A.L.; Ma, L.Q.; Wang, Z.W.; Zhang, D.S.; Li, K.; Zhang, Y.; Yi, X.J. Soil and water conservation in mining area based on ground surface subsidence control: Development of a high-water swelling material and its application in backfilling mining. *Environ. Earth Sci.* **2016**, *75*, 779. [[CrossRef](#)]
26. Fan, L.M. Some scientific issues in water-preserved coal mining. *J. China Coal Soc.* **2019**, *44*, 667–674.
27. Booth, C.J.; Bertsch, L.P. Groundwater geochemistry in shallow aquifers above longwall mines in Illinois, USA. *Hydrogeol. J.* **1999**, *7*, 561–575. [[CrossRef](#)]
28. Booth, C.J. Groundwater as an environmental constraint of longwall coal mining. *Environ. Geol.* **2006**, *49*, 796–803. [[CrossRef](#)]
29. Palchik, V. Localization of mining-induced horizontal fractures along rock layer interfaces in overburden: Field measurements and prediction. *Environ. Geol.* **2005**, *48*, 68–80. [[CrossRef](#)]
30. Liu, Y.; Yuan, S.C.; Yang, B.B.; Liu, J.W.; Ye, Z.Y. Predicting the height of the water-conducting fractured zone using multiple regression analysis and GIS. *Environ. Earth Sci.* **2019**, *78*, 422. [[CrossRef](#)]
31. Guo, W.B.; Zhao, G.B.; Lou, G.Z.; Wang, S.R. A new method of predicting the height of the fractured water-conducting zone due to high-Intensity longwall coal mining in China. *Rock Mech. Rock Eng.* **2019**, *52*, 2789–2802. [[CrossRef](#)]
32. Zhang, J.X.; Sun, Q.; Li, M.; Zhao, X. The mining induced seepage effect and reconstruction of key aquiclude strata during backfill mining. *Environ. Earth Sci.* **2019**, *38*, 590–601.
33. Huang, Q.X.; Lai, J.Q. Study on mechanical model of aquifuge beam supported by filling strip in the water preserved mining. *J. Min. Saf. Eng.* **2016**, *33*, 592–596.
34. Yu, Y.H.; Ma, L.Q. Application of Roadway Backfill Mining in Water-Conservation Coal Mining: A Case Study in Northern Shaanxi, China. *Sustainability* **2019**, *11*, 3719. [[CrossRef](#)]
35. Lv, K.; Deng, Z.G.; Xuan, Z.T.; Xiao, J.; Wu, X.Y. Surrounding rock failure mechanism of reserved roadway under superimposed mining and its control technology. *J. Min. Saf. Eng.* **2019**, *36*, 685–695.
36. Huang, Q.X. Research on roof control of water conservation mining in shallow seam. *J. China Coal Soc.* **2017**, *42*, 50–55.
37. Teerapharp, A.; Sontipee, A. A symplectic analytical approach for beams resting on multi-layered elastic foundations. *Int. J. Mech. Sci.* **2019**, *153–154*, 457–469.
38. Ma, L.Q.; Xu, Y.J.; Zhang, D.S.; Lai, X.P.; Huang, K.J.; Du, H.L. Characteristics of aquiclude and surface deformation in continuous mining and filling with wall system for water conservation. *J. Min. Saf. Eng.* **2019**, *36*, 34–40.

39. Guo, G.L.; Zhu, X.J.; Zha, J.F.; Wang, Q. Subsidence prediction method based on equivalent mining height theory for solid backfilling mining. *Trans. Nonferrous Met. Soc. China* **2014**, *24*, 3302–3308. [[CrossRef](#)]
40. Miao, X.X.; Huang, Y.L.; Ju, F.; Mao, X.B.; Guo, G.L.; Zhang, J.X. Strata movement theory of dense backfilling mining. *J. China Univ. Min. Technol.* **2012**, *41*, 863–867.
41. Cui, F.P.; Wu, Q.; Lin, Y.H.; Zeng, Y.F.; Zhang, K.L. Damage features and formation mechanism of the strong water inrush disaster at the daxing co mine, guangdong province, China. *Mine Water Environ.* **2018**, *37*, 1–5. [[CrossRef](#)]
42. Gao, R.; Yan, H.; Ju, F.; Mei, X.C.; Wang, X.L. Influential factors and control of water inrush in a coal seam as the main aquifer. *Int. J. Min. Sci. Technol.* **2018**, *28*, 187–193. [[CrossRef](#)]



© 2019 by the authors. Licensee MDPI, Basel, Switzerland. This article is an open access article distributed under the terms and conditions of the Creative Commons Attribution (CC BY) license (<http://creativecommons.org/licenses/by/4.0/>).